第 27 卷 第 4 期
2021 年 8 月

电化学
JOURNAL OF ELECTROCHEMISTRY

Vol. 27 No. 4
Aug. 2021

【Article】 **DOI**: 10.13208/j.electrochem.210329 **Http**://electrochem.xmu.edu.cn

DFT Study of $Ni_m@Pt_1Au_{n-m-1}$ (n=19, 38, 55, 79; m = 1, 6, 13, 19) Core-Shell ORR Catalyst

Wen-Jie Li[1], Dong-Xu Tian[1*], Hong Du[1], Xi-Qiang Yan[2*]

(*1. State Key Laboratory of Fine Chemicals, School of Chemical Engineering, Dalian University of Technology, Dalian 116024, Liaoning, China; 2. Guangdong Key Laboratory for Hydrogen Energy Technologies, Foshan University, Foshan 528000, Guangdong, China*)

Abstract: The slow kinetics of oxygen reduction reaction (ORR) limits the performance of low temperature fuel cells. Thus, it needs to design effective catalysts with low cost. Core-shell clusters (CSNCs) show promising activity because of their size-dependent geometric and electronic effects. The ORR activity trend of $Ni_m@Pt_1Au_{n-m-1}$ (n = 19, 38, 55, 79; m = 1, 6, 13, 19) was studied using the GGA-PBE-PAW methods. The adsorption configurations of *O, *OH and *OOH were optimized and the reaction free energies of four proton electron ($H^+ + e^-$) transfer steps were calculated. Using overpotential as a descriptor for the catalytic activity, $Ni_6@Pt_1Au_{31}$ was found to be the most active ORR catalyst. $Ni_1@Pt_1Au_{17}$, $Ni_{13}@Pt_1Au_{41}$, and $Ni_{19}@Pt_1Au_{59}$ had better activity than pure Pt clusters and Pt(111). Bader charge and DOS data indicate that the single Pt atom embedded on $Ni_m@Au_{n-m}$ can tune the electronic property of active site, and thus, significantly improve the activity. The present study showed that the single Pt atom embedded on $Ni_m@Au_{n-m}$ is a rational strategy to design effective core-shell ORR catalysts.

Key words: core-shell metal clusters; oxygen reduction reaction; density functional theory; overpotential; single atom catalysis

1 Introduction

The performance of low temperature fuel cells is controlled by the slow kinetics of oxygen reduction reaction (ORR), which needs to be overcome by designing effective catalysts with low cost[1-3]. Pt is the commonly used electrode material[4,5]. But the considerable overpotential[6-8] and high cost preventing its further commercial development. Thus it needs to design effective catalysts with low cost[9].

The most attractive advantage of core-shell nanoclusters (CSNCs) is that the core is made up of non-noble metals and an outer shell generally constituted precious metals. The electronic and geometric properties of CSNCs show many differences as compared with those of pure cluster and the bulk, which can make them become popular among cluster catalysis[10-12]. Most of the studies of core-shell are focused on late transition metals such as Fe, Co, Ni[13-15]. Jang et al. synthesized Fe@Pt CSNCs, which showed the surprising enhancement in activity by contrast with the Pt/C catalysts[16]. Wang et al. studied the core-shell Co@Pt nanoparticles (NPs) with different Pt shell thicknesses, and illustrated that Pt-skin (2 monolayers) covered NPs exhibited a 10-fold increment in activity compared to Pt/C catalysts. Chen and co-workers reported that Ni@Pt covered with a monolayer Pt shell showed a high activity[17].

Zhang et al. synthesized Pd@Pt with different Pt monolayers and found that the ORR activity could be tuned by changing the number of Pt monolayers[18].

Citation: Li W J, Tian D X, Du H, Yan X Q. DFT study of $Ni_m@Pt_1Au_{n-m-1}$ (n = 19, 38, 55, 79; m = 1, 6, 13, 19) core-shell ORR catalyst. *J. Electrochem.*, 2021, 27(4): 357-365.

Received: 2021-03-27, Revised: 2021-05-08. *Corresponding author, Tel: (86)13940816371,E-mail: tiandx@dlut.edu.cn, Tel: (86) 18718738074, E-mail: 965664856@qq.com

Park et al. found that Pd@Pt with 2 monolayers had the highest electrocatalytic activity for the ORR[19]. Zhang et al. reported that the ORR activity of alloy core@Pt could be tuned by varying the alloy core composition and found that 28% Au/72% Pd alloy@Pt had the highest activity[20]. Strasser and co-workers have synthesized Cu@Pt with different compositions ($Cu_{25}Pt_{75}$, $Cu_{50}Pt_{50}$, $Cu_{75}Pt_{25}$), and concluded that the Cu-rich $Cu_{75}Pt_{25}$ NPs was the most active ORR catalyst[21]. Zhang and co-worker found that $Pt_{0.8}@M_{0.2}$ (M = Pd, Re, Os, Ir, Ru, or Rh) enhanced the catalyst stability and further improved the ORR activity[22].

Theoretically CSNCs were studied by density functional theory (DFT) calculations[23]. Nanocluster models are very useful in explaining the stability and ORR activity of these nanoparticles. They can more effectively imitate the size-derived structure and the electronic effects, which is more effective than the periodic plate model. Cheng et al. reported that $Pt_{12}Mn$ and $Pt_{12}Fe$ clusters exhibited superior ORR activity[24]. 55-atom CSNCs consisting of late transition metals (Pd, Pt, Cu, Au, Fe, Co, Ni, Ru, etc.) were studied by Wang et al. and the results showed that Au, Pd, and Ag have good cooperation with Pt in improving catalytic activity[25]. Similarly, Shin et al. had a detailed study of 55-atom clusters, whose core was made up by late transition metal, which indicated that 3d transition metal cores put on a good performance in increasing ORR activity[26]. Furthermore, Akhil S. Nair et al. investigated 79-atoms cuboctahedral clusters and observed that $Ti_{19}@Pt_{60}$ is the most optimal catalyst[27]. Theoretical calculations and experimental results revealed that the main reason of improving catalytic activity is to weaken or strengthen adsorption energy of oxygenous species[28,29]. In order to search favorite core-shell structure combination, various metals have been previously studied. Late transition metals always show superior electrocatalytic performance for the ORR compared with early transition metals[30].

Although lots of work was performed, the design of low-cost, stable, and catalytically active core-shell materials needs more detailed experimental and computational work. In present work, a series of core-shell ORR clusters had been investigated by DFT. We studied the intermediate adsorption and gave a detailed analysis of ORR pathway. Using overpotential as a descriptor of ORR activity, we found that $Ni_6@Pt_1Au_{31}$ showed a superior ORR performance. And $Ni_1@Pt_1Au_{17}$, $Ni_6@Pt_1Au_{31}$, $Ni_{13}@Pt_1Au_{41}$ and $Ni_{19}@Pt_1Au_{59}$ also are possible promising electrocatalysts, exhibiting higher ORR catalyst activity than Pt (111). The present study would provide significant insights into for further searching for low-cost and high catalytic activity cathode catalysts.

2 Computational Details

The spin polarized DFT calculations were performed by using the Vienna Ab-initio Simulation Package (VASP)[31-33]. The electronic exchange and correlation effects were described using the generalized gradient approximation (GGA) within the Perdew-Burke-Ernzerhof (PBE) parametrization[34]. The ion-electron interactions were described by the projector augmented wave (PAW) method[35]. Kohn-Sham electronic wave functions were expanded in a plane wave basis set with a kinetic energy cut off of 400 eV. The cuboctahedral clusters are optimized in a 22 × 22 × 22 $Å^3$ supercell. The geometries were optimized using a conjugate-gradient method until the forces acting on each atom were less than 0.02 $eV \cdot Å^{-1}$[36]. The Brillouin zone is sampled with a Gamma (1 × 1 × 1) point. The periodic Pt(111) slab with 3 × 3 supercell and 4 atomic layers with a 20 Å vacuum. The model is sampled using the (5 × 5 × 1) K-point mesh. Grimme's D3 semiempirical dispersion correction method was considered for adsorption states[37,38]. Bader analysis proposed by Henkelman was adapted for studying the charge transfer[39].

Previous studies reported that oxygen reduction reaction takes place via peroxy intermediates on metal catalyst[40,41]. The oxygen reaction pathway was given by the elementary steps[23]:

$$O_2 + 4H^+ + 4e^- + * \rightarrow *OOH + 3H^+ + 3e^- \quad (1)$$

$$*OOH + 3H^+ + 3e^- \rightarrow *O + H_2O + 2H^+ + 2e^- \quad (2)$$

$$O* + H_2O + 2H^+ + 2e^- \rightarrow *OH + H_2O + H^+ + e^- \quad (3)$$

$$*OH + H_2O + H^+ + e- \rightarrow 2H_2O + * \quad (4)$$

The asterisk (*) represents an adsorption site. The adsorption energy (E_{DFT}) values of intermediates (*O, *OH and *OOH) are calculated using a water reference scheme, i.e.

$$2H_2O + * \rightarrow *OOH + 1.5H_2 \quad (5)$$

$$H_2O + * \rightarrow O* + H_2 \quad (6)$$

$$H_2O + * \rightarrow *OH + 0.5H_2 \quad (7)$$

Within the CHE model, we calculate free energies of the *O, *OH or *OOH intermediates at zero potential as $\Delta G = E_{DFT} + \Delta ZPE - T\Delta S$. ΔZPE is the zero point energy change, T is the temperature, and ΔS is the difference in entropy as can be seen in Table S1. The parameters about ΔZPE and $T\Delta S$ are derived from standard tables for gas phase molecules[32]. For adsorbates, the corresponding data were calculated from vibrational frequencies within the harmonic approximation. The vibrational contributions of atoms in the slab are neglected since they do not change appreciably during adsorption. Electronic structure, charge transfer, and binding energy analyses were performed to understand the activity trend of all the considered clusters[42].

3 Results and Discussion

3.1 Adsorption Properties and ORR Activity of Pt(111) and Pt_n (n = 19, 38, 55 and 79) Clusters

The geometric and electronic properties of nano-sized metal clusters are different from those of the bulk, which can make them attractive for ORR. In the present work, different-sized octahedron was used as a catalyst model, including 19-, 38-, 55- and 79-atom clusters (as shown in Figure 1), to understand the ORR activity trend. The 19-atom cluster consists of eight (111) faces, and the 38-, 55-, and 79-atom truncated octahedra are composed of eight (111) faces and six (100) faces as shown in Figure 1.

In the present work, the oxygen reaction pathway is given that it occurs via an associative mechanism through the peroxy intermediates. First, possible sites for the adsorption intermediates are considered and shown in Figure S1, and the most favorable adsorption sites of *O, *OH and *OOH are listed in Table S2. The four proton electron ($H^+ + e^-$) transfer steps of the associative mechanism are given in the computational details section. According to the BEP (Bell-Evans-Polanyi) principle, reaction free energy correlates the energy barriers. Thus, reaction free energy is used to explain the energetic trend of ORR. On the Pt(111) surface, the reaction free energy of four elementary steps was calculated to be -1.80, -1.96, -0.96 and -0.20 eV as listed in Table 1. The H_2O formation step was less preferred for efficient oxygen reduction. The rate-determining step (RDS) was the H_2O formation step with the calculated overpotential value of -0.20 eV.

Octahedral cluster consisting of (111) and (100) facets was used as a catalyst model to investigate the ORR activity trend. For Pt_n, the most stable adsorption position of *O, *OH and *OOH and the adsorption free energy are listed in Table S2. Compared to Pt(111), the adsorption strengths of adsorbed peroxy intermediates on Pt_n are stronger. The reaction free energy of elementary steps and overpotential on Pt_n (n = 19, 38, 55 and 79) clusters were calculated as shown in Table 1.

The free energy diagrams of elementary steps are shown in Figure 2. On Pt(111), all the reaction steps are downhill, implying a strongly exothermic reaction. But on Pt_n(n = 19, 38, 55 and 79) clusters, the

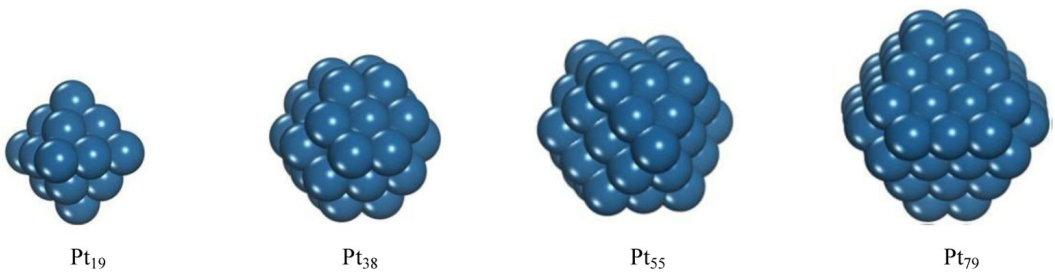

Figure 1 Geometry of Pt_n (n = 19, 38, 55, 79) (color on line)

Table 1 Free energy change of ORR elementary steps for Ptn and Pt(111)

System	ΔG_1/eV	ΔG_2/eV	ΔG_3/eV	ΔG_4/eV
Pt_{19}	-3.09	-0.95	-1.89	1.01
Pt_{38}	-2.47	-1.74	-1.14	0.42
Pt_{55}	-2.57	-1.67	-1.17	0.49
Pt_{79}	-2.23	-1.85	-1.08	0.24
Pt(111)	-1.80	-1.96	-0.96	-0.20

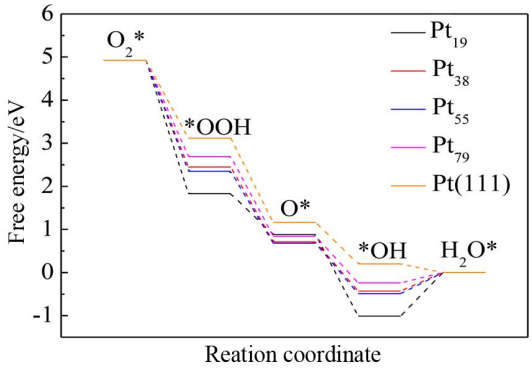

Figure 2 Free energy diagrams of ORR elementary steps over Pt_n and Pt(111) at U = 0 (color on line)

H_2O formation step is uphill, which needs to cross the energy barrier (overpotential). On Pt_{19}, Pt_{38}, Pt_{55} and Pt_{79} clusters, the energy barriers were calculated to be 1.01, 0.42, 0.49 and 0.24 eV, respectively. Relatively, they are not rational candidates for ORR, which arises from strong binding energy of *OH.

3.2 ORR Activity Trend of Core-Shell Ni_6@M_{32} Clusters

In order to design effective catalysts with low cost, we studied the activity trend of $Ni_6@M_{32}$ (M = Pt, Pd, Cu, Au, Ag). Favorable adsorption sites of *O, *OH and *OOH were investigated and the adsorption free energy was calculated as shown in Table S3. The reaction free energy of elementary steps was calculated as shown in Table 2. The free energy diagrams are shown in Figure 3. The H_2O formation step was found to be the RDS with the calculated overpotential values from Table 2.

For $Ni_6@Cu_{32}$, $Ni_6@Au_{32}$ and $Ni_6@Ag_{32}$ clusters, the overpotential values were calculated to be 0.91, 0.45 and 0.79 eV, respectively, showing a higher overpotential value than pure Pt_{38} cluster. But for $Ni_6@Pt_{32}$, and $Ni_6@Pd_{32}$ the overpotential values were calculated to be 0.01 eV, and 0.03 eV, respectively, which are lower than Pt_{38} cluster, highlighting the significance of core-shell structure in improving ORR activity. Taking $Ni_6@Pt_{32}$ as an example, the favorable adsorption site of $Ni_6@Pt_{32}$ is different from the pure Pt_{38} clusters. For $Ni_6@Pt_{32}$, it is the top site of Pt atom. However, it is the Pt-Pt bridge site over Pt_{38}. The adsorption free energy of OH on $Ni_6@Pt_{32}$ cluster

Table 2 Free energy change of ORR elementary steps for $Ni_6@M_{32}$ and Pt_{38} clusters

System	ΔG_1/eV	ΔG_2/eV	ΔG_3/eV	ΔG_4/eV
Pt_{38}	-2.47	-1.74	-1.14	0.42
$Ni_6@Pd_{32}$	-1.93	-1.91	-1.11	0.03
$Ni_6@Pt_{32}$	-2.10	-1.79	-1.02	0.01
$Ni_6@Cu_{32}$	-2.70	-1.63	-1.50	0.91
$Ni_6@Au_{32}$	-1.66	-1.58	-2.13	0.45
$Ni_6@Ag_{32}$	-2.58	-1.17	-1.96	0.79
Pt(111)	-1.80	-1.96	-0.96	-0.2

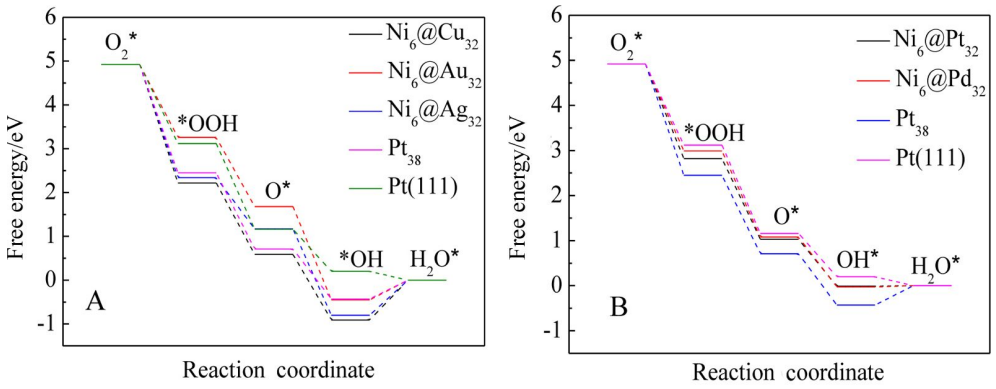

Figure 3 Free energy diagrams of ORR elementary steps over Pt_{38}, Pt(111) and (A) $Ni_6@Cu_{32}$, $Ni_6@Au_{32}$, $Ni_6@Ag_{32}$ and (B) $Ni_6@Pt_{32}$, $Ni_6@Pd_{32}$ (color on line)

was decreased by 0.41 eV than that on pure Pt_{38}, which leads to the smaller overpotential and higher ORR activity.

Bader charge was calculated to understand the reason of improved ORR performance. For $Ni_6@Pt_{32}$, the charge transfer from core to shell was 2.160 |e|, and for Pt_{38} the charge transfer from core to shell was calculated to be 1.078 |e|. Pt shell shows a remarkable electron-rich character, because of the obvious electronegativity difference between the Ni (1.91) and Pt (2.28) atoms[29,43]. Compared to pure Pt_{38} cluster, the charge accumulation on the Pt shell improves the activity of ORR by lowering the adsorption free energy of *OH.

3.3 ORR Activity Trend of $Ni_m@Pt_1Au_{n-m-1}$

Compared with the Pt (111), $Ni_6@M_{32}$ clusters are not favorable candidate catalysts for ORR. Ternary catalysts comprising Ni/NiO_x core and Pd shell with Pt cluster decoration on the surface (namely, Ni@Pd-Pt) in previous study were verified to have great ORR activity. Thus, cooperation with the third metal to tune the electronic properties is a good design strategy for ORR catalyst[44].

Taking 38-atom core-shell cluster as an example, the activity trend of $Ni_6@Pt_1Pd_{31}$, $Ni_6@Pt_1Cu_{31}$, $Ni_6@Pt_1Au_{31}$, and $Ni_6@Pt_1Ag_{31}$ was studied. Favorable adsorption sites of *O, *OH and *OOH were investigated and the adsorption free energy was calculated as shown in Table S4. The reaction free energy of $Ni_6@Pt_1N_{31}$(N = Pd, Cu, Au, Ag) are listed in Table 3.

The free energy diagrams can be seen in Figure 4. For $Ni_6@Pt_1Au_{31}$, the overpotential value was substantially decreased to -0.77 eV, and it was lowered by 1.22 eV compared to $Ni_6@Au_{32}$. From Table 3 we can see, relative to $Ni_6@M_{32}$ clusters, the overpotential values of $Ni_6@Pt_1Pd_{31}$, $Ni_6@Pt_1Cu_{31}$ and $Ni_6@Pt_1Ag_{31}$ were substantially lowered to -0.01, -0.38 and -0.21 eV, respectively. This result indicated that the single

Table 3 Free energy change of ORR elementary steps for $Ni_6@Pt_1N_{31}$(N = Pd, Cu, Ag, Au) and Pt_{38} clusters

System	ΔG_1/eV	ΔG_2/eV	ΔG_3/eV	ΔG_4/eV
Pt_{38}	-2.47	-1.74	-1.14	0.42
$Ni_6@Pt_1Pd_{31}$	-1.81	-1.76	-1.34	-0.01
$Ni_6@Pt_1Cu_{31}$	-2.05	-2.01	-0.49	-0.38
$Ni_6@Pt_1Au_{31}$	-1.52	-1.01	-1.61	-0.77
$Ni_6@Pt_1Ag_{31}$	-2.92	-0.23	-1.56	-0.21
Pt(111)	-1.80	-1.96	-0.96	-0.20

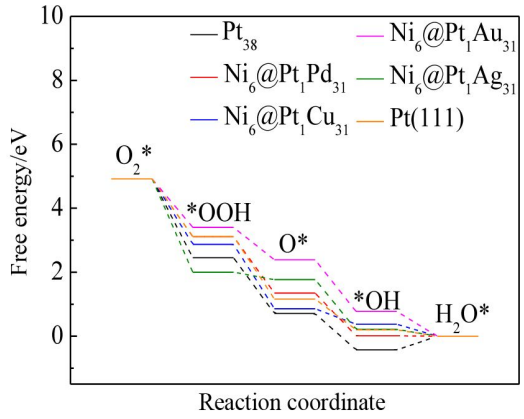

Figure 4 Free energy diagrams of ORR elementary steps over Pt single atom doped core-shell clusters at U = 0 (color on line)

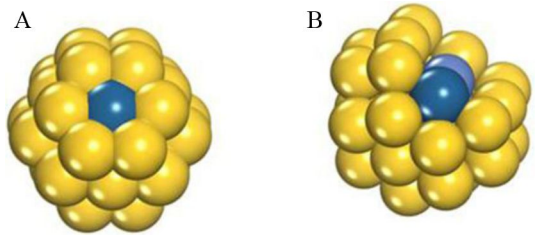

Figure 5 Schematic diagram of $Ni_6@Pt_1Au_{31}$, (A) geometry of $Ni_6@Pt_1Au_{31}$, (B) cutaway of $Ni_6@Pt_1Au_{31}$. Yellow represents Au shell, blue represents Pt and light blue represents Ni core atom.(color on line)

Pt atom embedded in Au shell of $Ni_6@Au_{32}$ significantly improved the activity of the core-shell material. The geometry of $Ni_6@Pt_1Au_{31}$ can be seen in Figure 5.

Accordingly, the activity trend of 19-, 55- and 79-atom clusters was further studied. Most favorable adsorption sites and adsorption free energies of ORR intermediates on 19-, 55- and 79-atom clusters are listed in Table S5. Reaction free energy of ORR elementary steps and the overpotential values are shown in Table S6, Figure S4. $Ni_1@Pt_1Au_{17}$, $Ni_6@Pt_1Au_{31}$, $Ni_{13}@Pt_1Au_{41}$ and $Ni_{19}@Pt_1Au_{59}$ are thought to be the favorable catalysts with the relatively lower overpotential values.

The Bader charge analysis of $Ni_m@Pt_1Au_{n-m-1}$ and $Ni_m@Au_{n-m}$ (n = 19, 38, 55, 79; m = 1, 6, 13, 19) was performed to understand the reason of improved performance and the results are summarized in Table S7. It can be seen that the single Pt atom in cooperation with Au shell of $Ni_m@Au_{n-m}$(n = 19, 38, 55, 79; m = 1, 6, 13, 19) can tune the electronic property of active site. $Ni_m@Pt_1Au_{n-m-1}$ shows a remarkable electron-rich character and results in a weaker binding strength. The partial density of states (PDOS) plots of OH adsorbed on $Ni_6@Pt_1Au_{31}$ and $Ni_6@Pt_{32}$ are shown in Figure 6. The d-state density near Fermi level is a significant decisive factor to influence the adsorption energy. Compared with $Ni_6@Au_{32}$, the Fermi level is more highly populated for adsorption site on $Ni_6@Pt_1Au_{31}$, leading to weaker adsorption strength and higher activity for ORR (Figure 5). PDOS data of 19-atom, 55-atom and 79atom are also given in Figure S5.

3.4 Stability Analysis of Clusters

The stability is an important factor to influence the ORR catalyst performance. In order to estimate the

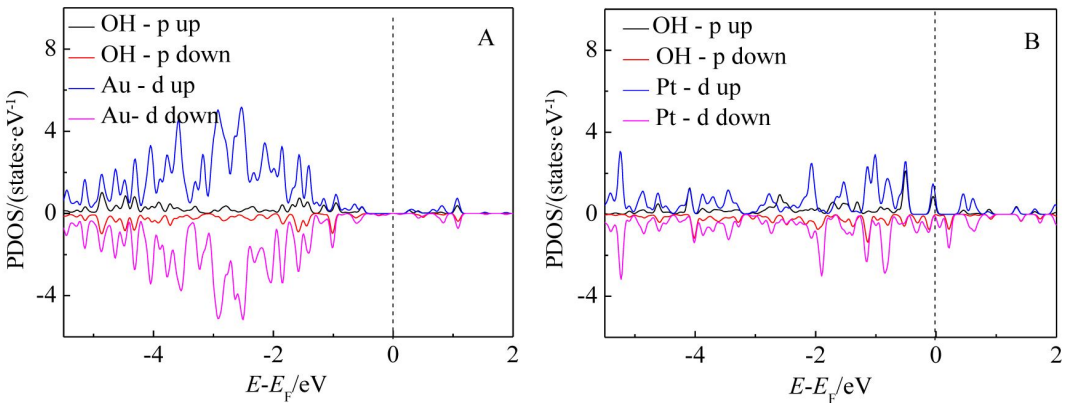

Figure 6 Partial density of states (PDOS) plots of OH on adsorption site of (A) $Ni_6@Au_{32}$ and (B) $Ni_6@Pt_1Au_{31}$ (color on line)

stability of the catalyst, we calculated the average formation energy of different core-shell clusters [27]. Average formation energy (E_f) of the clusters is calculated by using the following equation:

$$E_f = [(E(Ni_m@M_{n-m}) - m \times E_{Ni} + (n - m)\times E_M)]/n$$

(n represents the number of cluster atoms, m represents the number of shell atoms, M = Pt, Au; m = 1, 6, 13, 19; n = 19, 38, 55, 79). Smaller value of E_f indicates that the cluster is more stable.

From Figure 7, the introduction of Ni cores improved the stability compared with the pure Pt cluster, which is in agreement with the previous work[45]. For the 19, 55 79-atom clusters, the single Pt atom embedded in Au shell of $Ni_m@Au_{n-m}$ slightly improved the stability of clusters.

4 Conclusions

In summary, octahedron cluster was used as a catalyst model to study the activity trend of different-sized $Ni_m@Pt_1Au_{n-m-1}$(n = 19, 38, 55, 79; m = 1, 6, 13, 19) catalysts by GGA-PBE-PAW methods. The adsorption configurations of *O, *OH and *OOH were optimized and the reaction free energies were calculated. Using overpotential as a descriptor for the catalytic activity, the activity trend was found to be determined by the adsorption strength of *OH. $Ni_6@Pt_1Au_{31}$ is the most favorite catalyst for ORR. $Ni_1@Pt_1Au_{17}$, $Ni_{13}@Pt_1Au_{41}$, and $Ni_{19}@Pt_1Au_{59}$ have better ORR activities than pure Pt clusters and Pt(111). It was shown that a Pt atom embedded on $Ni_m@Au_{n-m}$ to form the $Ni_m@Pt_1Au_{n-m-1}$ is a rational strategy to design core-shell ORR catalysts. Bader charge and DOS data indicate that the single Pt atom embedded on $Ni_m@Au_{n-m}$ can tune the electronic property of active site, and significantly improve the activity. To some degree, $Ni_m@Pt_1Au_{n-m-1}$ fulfills the challenges of durability, activity and cost. The present study will provide significant insights into for further searching for low-cost and high ORR catalytic activity.

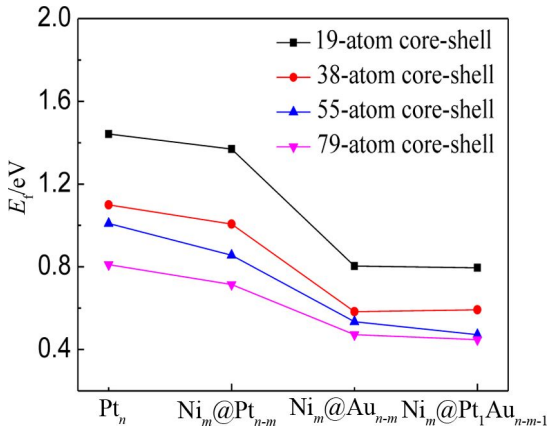

Figure 7 Average formation energy (E_f) of CSNCs(color on line)

Acknowledgements:

This work was supported by "the Fundamental Research Funds for the Central Universities" (DUT20ZD208) and Guangdong Key Laboratory for Hydrogen Energy Technologies (2018B030322005). The authors acknowledge the Supercomputer Center of Dalian University of Technology for providing computing resources.

References:

[1] Antolini E, Passos R R, Ticianelli E A. Electrocatalysis of oxygen reduction on a carbon supported platinum-vanadium alloy in polymer electrolyte fuel cells[J]. Electrochim. Acta., 2002, 48(3): 263-270.

[2] Gasteiger H A, Kocha S S, Sompalli B, Wagner F T. Activity benchmarks for Pt, Pt-alloy and non-Pt oxygen reduction catalysts for PEMFCs[J]. Appl. Catal. B - Environ., 2005, 56(1-2): 9-35.

[3] Debe M K. Electrocatalyst approaches and challenges for automotive fuel cells[J]. Nature, 2012, 486(7401): 43-51.

[4] Chen J, Lim B, Lee E P, Xia Y. Shape-controlled synthesis of platinum nanocrystals for catalytic and electrocatalytic applications[J]. Nano Today, 2009, 4(1): 81-95.

[5] Guo S J, Wang E K. Noble metal nanomaterials: Controllable synthesis and application in fuel cells and analytical sensors[J]. Nano Today, 2011, 6(3): 240-264.

[6] Koenigsmann C, Santulli A C, Gong K, Vukmirovic M B, Zhou W P, Sutter E, Wong S S, Adzic R R. Enhanced electrocatalytic performance of processed, ultrathin, supported Pd-Pt core-shell nanowire catalysts for the oxygen reduction reaction[J]. J. Am. Chem. Soc., 2011, 133(25): 9783-9795.

[7] Koenigsmann C, Sutter E, Chiesa T A, Adzic R R, Wong S S. Highly enhanced electrocatalytic oxygen reduction performance observed in bimetallic palladium-based nanowires prepared under ambient, surfactantless conditions[J]. Nano Lett., 2012, 12(4): 2013-2020.

[8] Sun S H, Zhang G X, Geng D S, Chen Y G, Li R Y, Cai M, Sun X L. A highly durable platinum nanocatalyst for proton exchange membrane fuel cells: multiarmed starlike nanowire single crystal[J]. Angew. Chem. Int. Ed., 2010, 50(2): 422-426.

[9] Yang P. Platinum-based electrocatalysts with core-shell nanostructures[J]. Angew. Chem. Int. Ed., 2011, 50(12): 2674-2676.

[10] Strasser P, Koh S, Anniyev T, Greeley J, Nilsson A. Lattice-strain control of the activity in dealloyed core-shell fuel cell catalysts[J]. Nature Chem., 2010, 2(6): 454-460.

[11] Guo S J, Zhang S, Sun S H. Tuning nanoparticle catalysis for the oxygen reduction reaction[J]. Angew. Chem. Int. Ed., 2013, 52(33): 8526-8544.

[12] Mani P, Srivastava R, Strasser P. Dealloyed PtCu core-shell nanoparticle electrocatalysts for use in PEM fuel cell cathodes[J]. J. Phys. Chem. C, 2012, 112(7): 2770-2778.

[13] Wang D L, Xin H L L, Hovden R, Wang H S, Yu Y C, Muller D A, Disalvo F J, Abrua H C. Structurally ordered intermetallic platinum-cobalt core-shell nanoparticles with enhanced activity and stability as oxygen reduction electrocatalysts[J]. Nat. Mater., 2012, 12(1): 81-87.

[14] Wang G X, Wu H M, Wexler D, Liu H K, Savadogo O. Ni@Pt core-shell nanoparticles with enhanced catalytic activity for oxygen reduction reaction[J]. J. Alloy. Compd., 2010, 503(1): L1-L4.

[15] Neergat M, Rahul R. Unsupported Cu-Pt core-shell nanoparticles: Oxygen reduction reaction (ORR) catalyst with better activity and reduced precious metal content[J]. J. Electrochem. Soc., 2012, 159(7): F234-F241.

[16] Jang J H, Lee E, Park J, Kim G, Hong S, Kwon Y U. Rational syntheses of core-shell Fex@Pt nanoparticles for the study of electrocatalytic oxygen reduction reaction[J]. Sci. Rep., 2013, 3: 2872.

[17] Chen Y M, Liang Z X, Yang F, Liu Y W, Chen S L. Ni-Pt core-shell nanoparticles as oxygen reduction electrocatalysts: Effect of Pt shell coverage[J]. J. Phys. Chem. C, 2011, 115(49): 24073-24079.

[18] Zhang Y F, Qin J, Leng D Y, Liu Q R, Xu X Y, Yang B, Yin F. Tunable strain drives the activity enhancement for oxygen reduction reaction on Pd@Pt core-shell electrocatalysts[J].J. Power Sources, 2021, 485: 229340.

[19] Park J, Zhang L, Choi S I, Roling L T, Lu N, Herron J A, Xie S F, Wang J G, Kim M J, Mavrikakis M, Xia Y N. Atomic layer-by-layer deposition of platinum on palladium octahedra for enhanced catalysts toward the oxygen reduction reaction[J]. ACS Nano, 2015, 9(3): 2635-2647.

[20] Zhang L, Iyyamperumal R, Yancey D F, Crooks R M, Henkelman G. Design of Pt-shell nanoparticles with alloy cores for the oxygen reduction reaction[J]. ACS Nano, 2013, 7(10): 9168-9172.

[21] Strasser P, Koh S, Anniyev T, Greeley J, More K, Yu C, Liu Z, Kaya S, Nordlund D, Ogasawara H, Toney M F, Nilsson A. Lattice-strain control of the activity in dealloyed core-shell fuel cell catalysts[J]. Nat. Chem., 2010, 2(6): 454-460.

[22] Zhang J L, Vukmirovic M B, Sasaki K, Nilekar A U, Mavrikakis M, Adzic R R. Mixed-metal Pt monolayer electrocatalysts for enhanced oxygen reduction kinetics[J]. J. Am. Chem. Soc., 2005, 127(36): 12480-12481.

[23] Nörskov J K, Rossmeisl J, Logadottir A, Lindqvist L, Kitchin J R, Bligaard T, Jónsson H. Origin of the overpotential for oxygen reduction at a fuel-cell cathode[J]. J. Phys. Chem. B, 2004, 108(46): 17886-17892.

[24] Cheng D J, Qiu X G, Yu H Y. Enhancing oxygen reduction reaction activity of Pt-shelled catalysts via subsurface alloying[J]. Phys. Chem. Chem. Phys., 2014, 16(38): 20377-20381.

[25] Wang L L, Johnson D D. Predicted trends of core-shell preferences for 132 late transition-metal binary-alloy nanoparticles[J]. J. Am. Chem. Soc., 2009, 131(39): 14023-14029.

[26] Shin J, Choi J H, Cha P R, Kim S K, Kim I, Lee S C, Jeong D S. Catalytic activity for oxygen reduction reaction on platinum-based core-shell nanoparticles: All-electron density functional theory[J]. Nanoscale, 2015, 7(38): 15830-15839.

[27] Nair A, Pathak B. Computational screening for ORR activity of 3d transition metal based M@Pt core-shell clusters[J]. J. Phys. Chem. C, 2019, 127(6): 3634-3644.

[28] Greeley J, Stephens I E L, Bondarenko A S, Johansson T P, Hansen H A, Jaramillo T F, Rossmeisl J, Chorkendorff I, Nørskov J K. Alloys of platinum and early transition metals as oxygen reduction electrocatalysts[J]. Nat. Chem., 2009, 1(7): 552-556.

[29] Bligaard T, Norskov J K, Dahl S, Matthiesen J, Christensen C H, Sehested J. The Brnsted-Evans-Polanyi relation and the volcano curve in heterogeneous catalysis[J]. J. Catal., 2004, 224(1): 206-217.

[30] Sobrinho D G, Nomiyama R K, Chaves A S, Piotrowski M J, Silva J. Structure, electronic, and magnetic properties of binary Pt_nTM_{55-n} (TM = Fe, Co, Ni, Cu, Zn) nanoclusters: A density functional theory investigation[J]. J. Phys. Chem. C, 2015, 119(27): 15669-15679.

[31] Kresse G, Hafner J. Ab initio molecular-dynamics simulation of the liquid-metal-amorphous-semiconductor tran-

sition in germanium[J]. Phys. Rev. B, 1994, 49(20): 14251-14269.

[32] Kresse G G, Furthmüller J J. Efficient iterative schemes for ab initio total-energy calculations using a plane-wave basis set[J]. Phys. Rev. B, 1996, 54(16): 11169-11186.

[33] Perdew J P, Yue W. Accurate and simple density functional for the electronic exchange energy: Generalized gradient approximation[J]. Phys. Rev. B, 1986, 33(12): 8800-8802.

[34] Perdew J P, Chevary J A, Vosko S H, Jackson K A, Pederson M R, Singh D J, Fiolhais C. Erratum: Atoms, molecules, solids, and surfaces: Applications of the generalized gradient approximation for exchange and correlation[J]. Phys. Rev. B, 1993, 46(11): 6671-6687.

[35] Kresse G, Joubert D. From ultrasoft pseudopotentials to the projector augmented-wave method[J]. Phys. Rev. B, 1999, 59(3): 1758-1775.

[36] Teter M P, Payne M C, Allan D C. Solution of Schrödinger's equation for large systems[J]. Phys. Rev. B, 1989, 40(18): 12255-12263.

[37] Grimme S. Accurate description of van der Waals complexes by density functional theory including empirical corrections[J]. J. Comput. Chem., 2004, 25(12): 1463-1473.

[38] Lee K, Murray Amonn D, Kong L, Lundqvist B I, Langreth D C. A higher-accuracy van der waals density functional[J]. Phys. Rev. B, 2010, 82(8): 081101.

[39] Henkelman G, Arnaldsson A, Jónsson H. A fast and robust algorithm for Bader decomposition of charge density[J]. Comput. Mater. Sci., 2006, 36(3): 354-360.

[40] Grgur B N, Markovi N M, Ross P N. Temperature-dependent oxygen electrochemistry on platinum low-index single crystal surfaces in acid solutions[J]. Can. J. Chem., 1997, 75(11): 1465-1471.

[41] Blizanac B B, Lucas C A, Gallagher M E, Arenz M, Ross P N, Markovic N M. Anion adsorption, CO oxidation, and oxygen reduction reaction on a Au(100) surface: The pH effect[J]. J. Phys. Chem. B, 2004, 108(2): 625-634.

[42] Wang L, Zeng Z H, Ma C, Liu Y F, Giroux M, Chi M F, Jin J, Greeley J, Wang C. Plating precious metals on non-precious metal nanoparticles for sustainable electrocatalysts[J]. Nano Lett., 2017, 17(6): 3391-3395.

[43] Fang P P, Duan S, Lin X D, Anema J R, Li J F, Buriez O, Ding Y, Fan F R, Wu D Y, Ren B, Wang Z L, Amatore C, Tian Z Q. Tailoring Au-core Pd-shell Pt-cluster nanoparticles for enhanced electrocatalytic activity[J]. Chem. Sci., 2011, 2(3): 531-539.

[44] Dinesh B, Jyh-Pin C, Che Y, Hu A, Yang Y T, Chen T Y. Programming ORR Activity of Ni/NiO_x@Pd electrocatalysts via controlling depth of surface-decorated atomic Pt clusters[J]. ACS Omega, 2018, 3(8): 8733-8744.

[45] Wang H, An W. Promoting the oxygen reduction reaction with gold at step/edge sites of Ni@AuPt core-shell nanoparticles[J]. Catal. Sci. Technol., 2017, 7(3): 596-606.

ORR 催化剂 $Ni_m@Pt_1Au_{n-m-1}$(n = 19, 38, 55, 79; m = 1, 6, 13, 19)的密度泛函研究

李文杰[1],田东旭[1*],杜　红[1],燕希强[2*]

(1. 大连理工大学化工学院,精细化工国家重点实验室,辽宁 大连 116024;
2. 佛山(云浮)氢能产业与新材料发展研究院,广东省氢能技术重点实验室,广东 佛山 528000)

摘要: 燃料电池的阴极反应的反应动力学速率非常慢,限制了燃料电池技术的发展。因此,寻找低成本、高活性的氧还原催化剂具有重要的意义。多元金属核壳团簇表现出优良的氧还原活性。在本文中,以原子个数为 19、38、55 和 79 的八面体团簇作催化剂模型,采用密度泛函理论(GGA-PBE-PAW)方法,研究了一系列不同尺寸核壳 $Ni_m@M_{n-m}$ (n = 19, 38, 55, 79; m = 1, 6, 13, 19; M = Pt, Pd, Cu, Au, Ag)团簇催化剂的活性规律。优化 *O、*OH 和 *OOH 吸附中间体结构,计算了吸附自由能和反应吉布斯自由能,以超电势为催化活性的描述符,研究了单原子 Pt 嵌入 $Ni_m@Au_{n-m}$ 团簇的活性规律。结果表明,$Ni_6@Pt_1Au_{31}$ 具有最好的 ORR 活性,并且 $Ni_1@Pt_1Au_{17}$、$Ni_6@Pt_1Au_{31}$、$Ni_{13}@Pt_1Au_{41}$、$Ni_{19}@Pt_1Au_5$ 表现出比 Pt_{38} 团簇以及 Pt(111)表面更高的催化活性。Bader 电荷和态密度分析表面,核壳之间的电荷转移以及单原子 Pt 嵌入 $Ni_m@Au_{n-m}$ 表面,改变了吸附位的电子性质,降低了 *OH 的吸附强度,提高了 ORR 活性。单原子 Pt 嵌入 $Ni_m@Au_{n-m}$ 表面可能是一种合适的多元金属核壳 ORR 催化剂设计策略。

关键词: 核壳金属团簇;氧还原反应;密度泛函理论;超电势;单原子催化